catalysts

MDPI

Article

Effect of Operating Temperature, Pressure and Potassium Loading on the Performance of Silica-Supported Cobalt Catalyst in CO_2 Hydrogenation to Hydrocarbon Fuel

Rama Achtar Iloy and Kalala Jalama *

Department of Chemical Engineering, Doornfontein Campus, University of Johannesburg, Doornfontein 2028, Johannesburg, South Africa; achtar2006@yahoo.fr

* Correspondence: kjalama@uj.ac.za

Received: 31 August 2019; Accepted: 10 September 2019; Published: 26 September 2019

Abstract: Potassium (1–5 wt.%)-promoted and unpromoted Co/SiO_2 catalysts were prepared by impregnation method and characterized by nitrogen physisorption, temperature-programmed reduction (TPR), CO_2 temperature-programmed desorption (TPD), X-ray diffraction (XRD) and X-ray photoelectron spectroscopy (XPS) techniques. They were evaluated for CO_2 hydrogenation in a fixed bed reactor from 180 to 300 °C within a pressure range of 1–20 bar. The yield for hydrocarbon products other than methane (C_{2+}) was found to increase with an increase in the operating temperature and went through a maximum of approximately 270 °C. It did not show any significant dependency on the operating pressure and decreased at potassium loadings beyond 1 wt.%. Potassium was found to enhance the catalyst ability to adsorb CO_2, but limited the reduction of cobalt species during the activation process. The improved CO_2 adsorption resulted in a decrease in surface H/C ratio, the latter of which enhanced the formation of C_{2+} hydrocarbons. The highest C_{2+} yield was obtained on the catalyst promoted with 1 wt.% of potassium and operated at an optimal temperature of 270 °C and a pressure of 1 bar.

Keywords: CO_2 hydrogenation; cobalt; potassium; pressure; temperature

1. Introduction

The promoting capabilities of alkali metals, namely potassium, have been investigated for a variety of catalysts and reactions, including steam reforming of bioethanol [1], water gas shift [2], N_2O decomposition [3], Fischer-Tropsch synthesis (FTS) [4–6] and CO_2 hydrogenation [7–11]. One of the earliest studies on the use of potassium as a promoter for the catalyst used in CO_2 hydrogenation to hydrocarbons is that of Russell and Miller [12]. They investigated several copper-activated cobalt catalysts at atmospheric pressure from 448 to 573 K with H_2/CO_2 ratio varied from 2 to 3. All the catalysts mainly produced methane and liquid hydrocarbons were observed only after potassium addition to the catalyst in the form of either potassium carbonate or phosphate. Potassium was believed to selectively poison methane forming centres, and therefore, promote methylene radicals polymerization by the repression of the competitive hydrogenation reaction. Similarly, Owen et al. [13] studied the effect of potassium, along with that of lithium and sodium, on the performance of Co/SiO_2 catalysts. The catalytic testing was carried out at 643 K, atmospheric pressure and using an H_2/CO_2 ratio of 3. They showed that with an alkali loading as low as 1 wt.%, the products distribution shifts towards longer chain hydrocarbons. Furthermore, C_2 and C_3 olefins, which did not form over the unpromoted catalyst, were detected in relatively significant amounts over the promoted catalysts. The authors attributed this behaviour to the ability of potassium to enhance the surface to molecule charge

transfer, resulting in increased CO and reduced hydrogen binding strength. These findings were further corroborated by a more recent investigation by Shi et al. [8] on a $CoCu/TiO_2$ system containing 1.5–3.5 wt.% K. Using CO_2 temperature-programmed desorption, the authors were able to link an improved yield of liquid hydrocarbons (C_{5+}) to the increased CO_2 adsorption capacity of the catalyst, when loaded with potassium.

It appears that potassium has an enormous potential in the conversion of CO_2 to liquid hydrocarbons. To derive most of the benefit from this promoter, the study of its effect on the reaction must be integrated with that of the effect of operating conditions. Most studies have reported the effect of potassium on cobalt-based catalysts under pre-selected operating conditions that were not optimized. Hence, the present study aims at systematically evaluating the promoting effect of potassium on a Co/SiO_2 system used in CO_2 hydrogenation under optimized temperature and pressure conditions.

2. Results and Discussion

2.1. Surface Area and Porosity

The information on the surface area and porosity of the catalysts investigated is presented in Table 1. The data show that cobalt incorporation into the silica support results in a significant drop in the surface area from 186.6 to 133.1 m^2/g. This behaviour is generally explained by the growth of cobalt oxide particles within the pores of the support during catalyst calcination, leading to some level of pore obstruction. This agrees well with the pore volume data, which show a decrease from 1.5 to 1.0 cm^3/g. The introduction of potassium, in amounts above 3% in the catalyst, further amplifies this phenomenon.

Table 1. Surface area and porosity data.

Sample	BET Surface Area (m^2/g)	Pore Volume (cm^3/g)	Pore Diameter (nm)
SiO_2	186.6	1.5	31.2
$15\%Co/SiO_2$	133.1	1.0	30.2
$15\%Co\text{-}1\%K/SiO_2$	137.8	1.2	33.4
$15\%Co\text{-}3\%K/SiO_2$	123.4	1.1	35.5
$15\%Co\text{-}5\%K/SiO_2$	70.0	0.8	45.1

2.2. X-ray Diffraction

Figure 1 shows the XRD patterns of unpromoted and promoted catalysts before and after reduction. All the unreduced catalysts showed diffraction peaks at 2θ values of approximately 18°, 30°, 36.6°, 39°, 44.5°, 55.3°, 60° and 65°, attributed to Co_3O_4 [14].

After catalysts reduction, the diffraction peaks for Co_3O_4, which were present in the unreduced catalysts disappeared (Figure 1b). The only visible peaks are those of the lower oxide of cobalt (CoO) at 42.4° and metallic cobalt at 44.5°.

The Scherrer equation was used to calculate the average crystallite sizes of cobalt species in the catalyst, using two theta values of 36.6°, 42.4° and 44.5° for Co_3O_4, CoO and Co respectively. The data are reported in Table 2. Although there is no observable trend in the data with respect to Co_3O_4 and Co, it appears that the average crystallite size for CoO decreases with increasing potassium loading in the catalyst. This suggests that potassium controls the size of CoO in the catalyst.

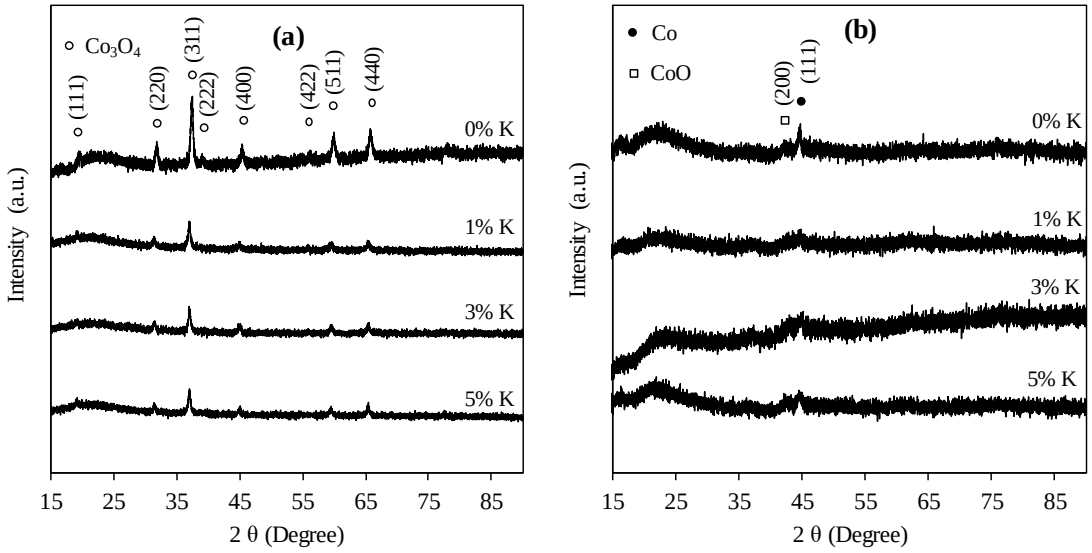

Figure 1. XRD patterns for unpromoted and potassium-promoted 15%Co/SiO_2 catalysts: (**a**) Before reduction, and (**b**) after reduction.

Table 2. The particle size of the calcined catalysts.

Catalyst	Freshly Calcined [a]	Reduced and Passivated [a]	
	Co_3O_4	CoO	Co
15%Co/SiO_2	18.16	9.36	9.44
15%Co-1%K/SiO_2	23.52	7.30	7.34
15%Co-3%K/SiO_2	24.35	6.70	6.72
15%Co-5%K/SiO_2	19.13	2.46	8.85

[a] Particle size in nm.

2.3. Temperature-Programmed Reduction (TPR)

The effect of potassium addition on the reducibility of silica-supported cobalt catalysts was investigated using TPR analysis. TPR profiles of various potassium-promoted catalysts, along with that of the unpromoted sample are presented in Figure 2. For the unpromoted catalyst, an early and slow reduction process was observed from ca. 170 °C. It became significant from ca. 290 °C, where a fast reduction peak was observed to start and went through a maximum at 365 °C. Subsequent overlapping reduction peaks, with respective maxima at ca. 395, 425 and 466 °C, were also observed. These peaks can be attributed to a two-step reduction of Co_3O_4 species in the catalyst to CoO and Co^0. The presence of more than two peaks observed for this reduction process could indicate that not all the cobalt species in the catalyst underwent reduction at the same time. For example, as N_2 adsorption data suggest some level of pore obstruction in the catalyst, it is possible that some cobalt species only got reduced after the reduction of some of those that blocked some pores. Adding potassium to the catalyst reduced the reducibility of cobalt species as per the following observations: (i) The reduction temperatures for the catalysts shifted to higher values. For example, the start of the reduction process moved from 170 °C for the unpromoted catalyst to 210 and 255 °C for catalysts containing 1% and 3–5% K respectively; (ii) the area under the TPR profile below 500 °C decreased, indicating lower degree of catalyst reduction as the amount of potassium increased in the catalyst and (iii) the formation of cobalt species in strong interaction with the support, as shown by a broad reduction peak, with a maximum at ca. 512 °C, observed in the catalyst containing 5% K. The negative effect of potassium on the reduction of cobalt catalyst was also reported by Jacobs et al. [6] who found that (0.5–5%) K shifted

the reduction peak temperatures to higher values and lowered the extent of catalyst reduction. This suggests that potassium interacts with the cobalt species and possibly the silica support [15].

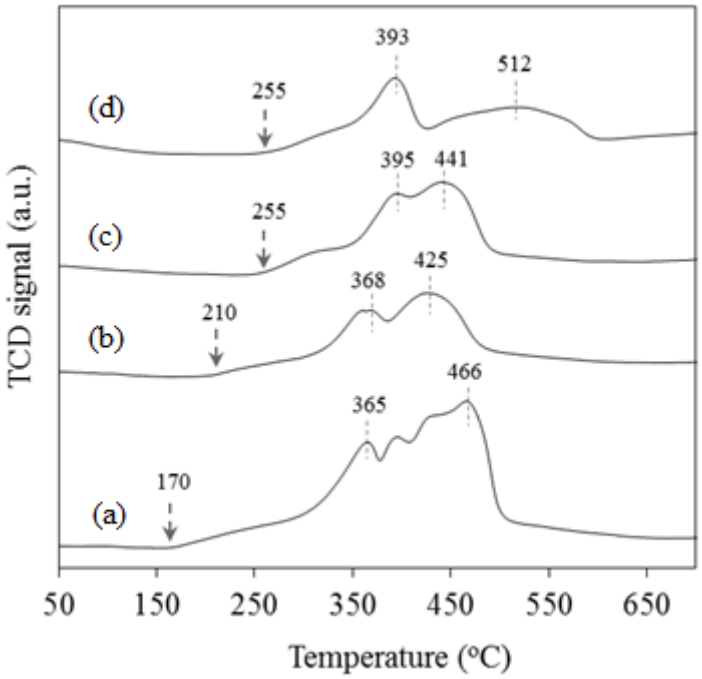

Figure 2. TPR profiles for (**a**) 15%Co/SiO_2, (**b**) 15%Co-1%K/SiO_2, (**c**) 15%Co-3%K/SiO_2, and (**d**) 15%Co-5%K/SiO_2.

2.4. CO_2 Temperature-Programmed Desorption (CO_2-TPD)

CO_2-TPD profiles for 15%Co/SiO_2 and 15%Co-1%K/SiO_2 are presented in Figure 3. Both catalysts showed two desorption peaks, with the first one centred at 65 °C with near-identical areas. This low-temperature peak can be attributed to the desorption of physically adsorbed CO_2. A second peak, observed for each catalyst, was attributed to the desorption of chemisorbed CO_2 and was used as an indication of the strength and amounts of basic sites in the catalyst. As expected, the data show that the addition potassium to the catalyst increases the strength and amounts of basic sites in the catalyst. This is indicated by the large and extended CO_2 desorption peak, which goes through its maximum at ca. 187 °C, compared to a corresponding small peak, with a maximum at ca. 134 °C, for the unpromoted catalyst. These data agree with earlier studies [8,16] that also reported an improvement in CO_2 adsorption in cobalt-based catalyst upon potassium addition.

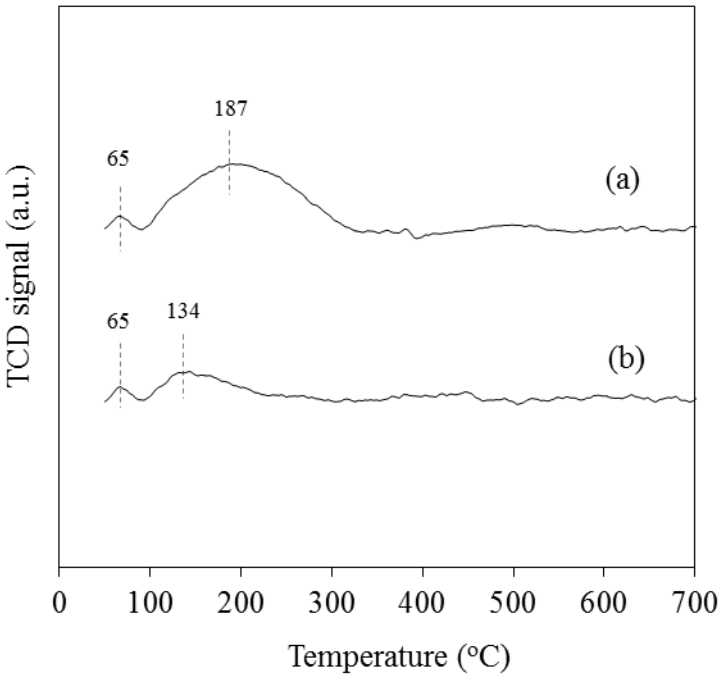

Figure 3. CO_2-TPD profiles of (**a**) 15%Co-1%K/SiO_2 and (**b**) 15%Co/SiO_2.

2.5. X-ray Photoelectron Spectroscopy (XPS)

XPS spectra, in the Co 2p region, for calcined and activated catalysts are shown in Figure 4.

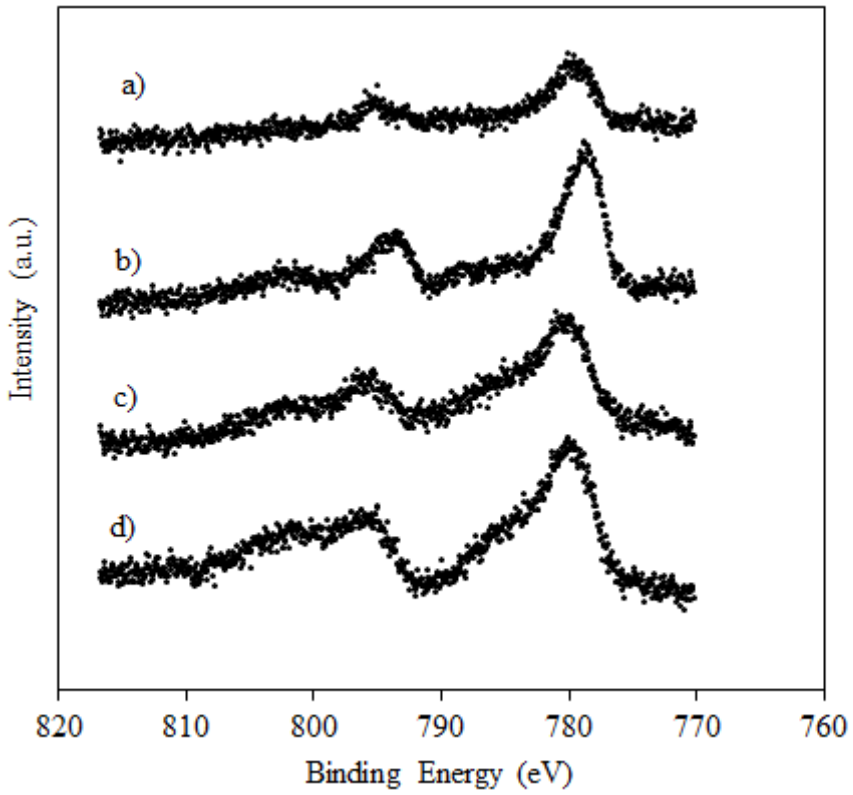

Figure 4. XPS data for calcined catalysts (**a**) 10%Co/SiO_2-calc., (**b**) 10%Co/1%K/SiO_2-calc.; and reduced catalysts (**c**) 10%Co/SiO_2-red., (**d**) 10%Co/1%K/SiO_2-red.

The Co $2p_{1/2}$ and $2p_{3/2}$ peaks for the calcined and unpromoted catalyst were respectively observed at ca. 795.2 and 779.6 eV and are characteristic of Co_3O_4 [14,17], in agreement with XRD data, discussed in Section 2.2. A shift to lower binding energies can be observed for Co $2p_{1/2}$ (to 793.5 eV) and $2p_{3/2}$ (to 778 eV) following catalyst promotion with potassium. This suggests an electronic donation by potassium as also observed by other studies, where potassium was added to Co/Al_2O_3 [18] and Pd/Co_3O_4 and Co_3O_4 [19] catalysts.

Spectra of reduced catalysts (Figure 4c,d) display features of CoO with broader Co $2p_{1/2}$ and $2p_{3/2}$ peaks and increased intensities of the shake-up satellite features [17,20]. They look similar for both the unpromoted and the potassium-promoted catalysts. These findings indicate that the electronic properties of cobalt in the catalyst were modified by potassium during the calcination process, not during catalyst reduction, causing a different reduction behaviour for the promoted catalyst.

2.6. Catalyst Testing

2.6.1. Effect of Temperature

In order to study the effect of temperature, CO_2 hydrogenation was carried out over a 15%Co-3%K/SiO_2 catalyst at atmospheric pressure from 180 to 300 °C. The temperature dependency of CO_2 conversion and its corresponding Arrhenius plot are reported in Figure 5. As expected, the CO_2 conversion continuously increased from 0.6 to 18.4% as the temperature was raised from 180 to 300 °C, in agreement with other earlier studies [21–23].

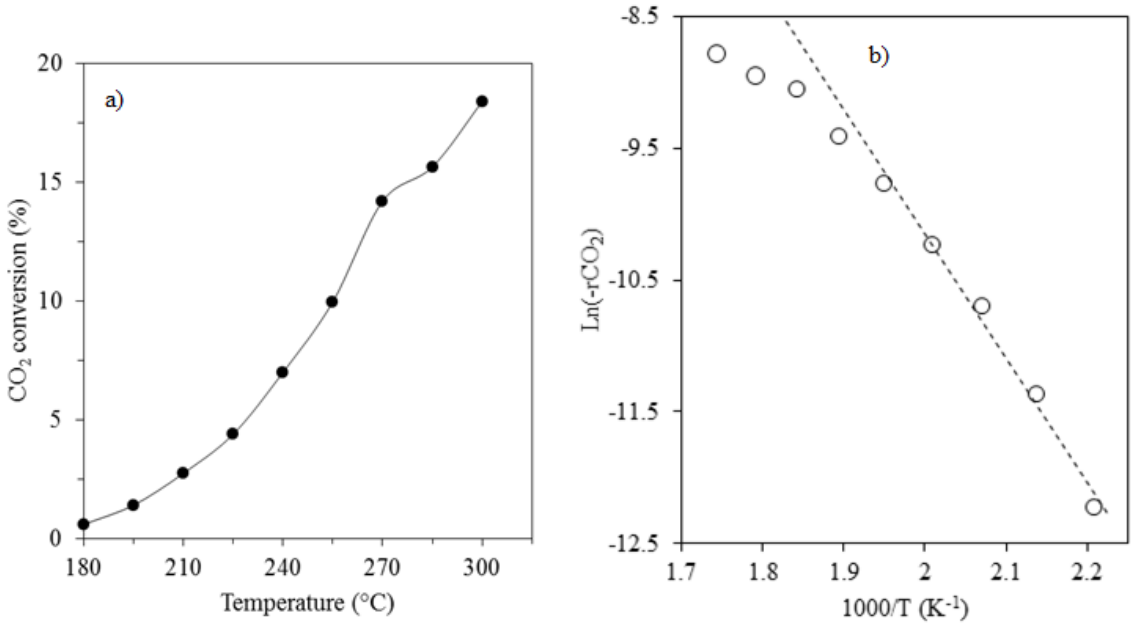

Figure 5. CO_2 conversion during hydrogenation vs. reaction temperature (1 bar, SV = 0.92 NL/g_{cat}/h, H_2/CO_2 = 3.1/1): (**a**) CO_2 conversion vs. temperature; (**b**) Arrhenius plot (Ea = 78 kJ/mol).

From the Arrhenius plot, activation energy of 78 kJ/mol was obtained in a temperature range of 180 to 240 °C. A marked curvature in the Arrhenius plot can be observed at temperatures above 240 °C, suggesting that the catalyst surface underwent some changes, possibly including deactivation by carbon [23]. For comparison, activation energies reported by earlier studies involving cobalt catalysts for CO_2 hydrogenation are summarised in Table 3.

The value of the activation energy obtained in this study is similar to most of those reported in earlier studies. Exceptions can be noticed for the data reported by Weatherbee and Bartholomew [23], who reported activation energies of 93 and 171 kJ/mol over 15%Co/SiO2 at 1 and 10 bar respectively.

The effect of the operating temperature on products selectivity and yields is summarized in Figure 6. The methane selectivity showed relatively little dependency on temperature from 180 to 225 °C, but continuously increased from 240 to 300 °C, while the selectivity to CO decreased almost linearly with increasing temperature (Figure 6a). Both C_2-C_4 and C_{5+} selectivities increased as the temperature was raised and went through a maximum at 240 °C before decreasing. Figure 6c shows that up to 270 °C, the yields for C_{2+}, CH_4 and CO all increased with the rise in temperature, with the yield of CO remaining the highest of the three. The yield of methane and C_{2+} hydrocarbons were similar up to 240 °C, above which the yield of methane quickly surpassed that of C_{2+} in an exponential manner.

Table 3. The activation energy for CO_2 hydrogenation over cobalt catalysts.

Catalyst	H_2/CO_2	P (atm.)	T (°C)	Ea (kJ/mol)	References
15%Co/3%K/SiO_2	3/1	1	180–240	78	This work
Pristine Co	4/1	1	207–237	77	[24]
100% Co	4/1	1	190–230	79	[25]
4.5%Co/S1 *	4/1	1	210–260	79	[25]
4.6%Co/S3 *	4/1	1	200–240	76	[25]
15%Co/SiO_2	4/1	1	183–203	93	[23]
15%Co/SiO_2	4/1	11	180–222	171	[23]
3%Co/SiO_2	4/1	1	227–277	79	[23]

* S1 and S3 are carbon supports obtained from saran copolymer. The difference between the two is in the burn-off percentage, i.e., 0 and 20% for S1 and S3 respectively [26].

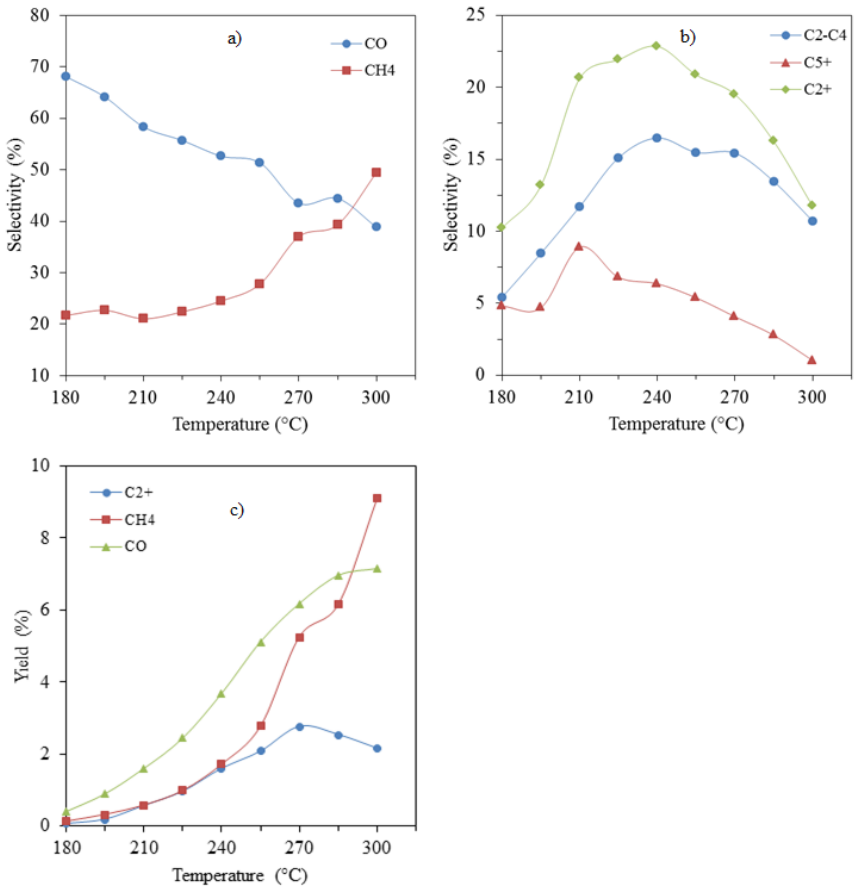

Figure 6. Effect of temperature on products selectivity: (**a**) CH_4 and CO; (**b**) C_{2+} hydrocarbons; and products yields: (**c**) C_{2+}, CH_4 and CO.

The rise in CO yield flattened off around 285 °C and was surpassed by the fast-rising yield of methane around 290 °C. The C_{2+} yield went through a maximum at 270 °C, indicating that, above this temperature, the reaction is turning into a preferential methanation process.

The mechanism of CO_2 hydrogenation to hydrocarbons is still subject of some controversies. However, since CO formed during CO_2 hydrogenation, it is most likely that hydrocarbons formed via a typical Fischer-Tropsch mechanism. Indeed, this is a plausible explanation, since some studies [27–29] have shown that, in the presence of CO, on cobalt-based catalysts, CO_2 behaves like an inert gas and only reacts when CO is depleted. Also, the rapid increase in methane yields with the temperature at values above 240 °C is typical to FT reaction [22,23]. An operating temperature of 270 °C was selected as optimal for the rest of the study.

2.6.2. Effect of Pressure

The effects of pressure on CO_2 conversion, and products selectivities and yields are reported in Figure 7. An increase in operating pressure, from 1 to 15 bar, resulted in an increase in CO_2 conversion. As can be seen from Figure 7a, the CO_2 conversion measured at 1 bar was ca. 12.5%; it increased to ca. 21%, 22%, and 27% when the pressure was increased to 5, 10 and 15 bar, respectively. Further increase in the operating pressure to 20 bar resulted in a slight decrease of CO_2 conversion to ca. 26%. The increase in CO_2 conversion with the operating pressure from 1 to 15 bar was expected because of an increase in reactants partial pressures. However, the decrease in CO_2 conversion observed when the operating pressure was increased from 15 to 20 bar was not expected; it is possible that some CO_2 or reaction intermediate species irreversibly adsorbed on the catalyst surface, blocking some active sites.

An increase in operating pressure from 1 to 5 bar significantly decreased the selectivities to CO and C_{2+} hydrocarbons from ca. 48% and 21% to 8% and 11%, respectively (Figure 7b). Further increase in pressure only resulted in slight decreases in CO and C_{2+} hydrocarbons selectivities. An opposite behaviour was observed for CH_4 selectivity, which increased from 30 to 81% when the operating pressure was increased from 1 to 5 bar. Further increase in operating pressure resulted in a relatively slight increase in CH_4 selectivity. Similar trends can be observed for CO and CH_4 yields as a function of the operating pressure (Figure 7c); however, the C_{2+} yield was not significantly affected by changes in operating pressure. It remained between 2.1% and 2.7% over the range of pressure used. Under these conditions, operating at 1 bar is optimal.

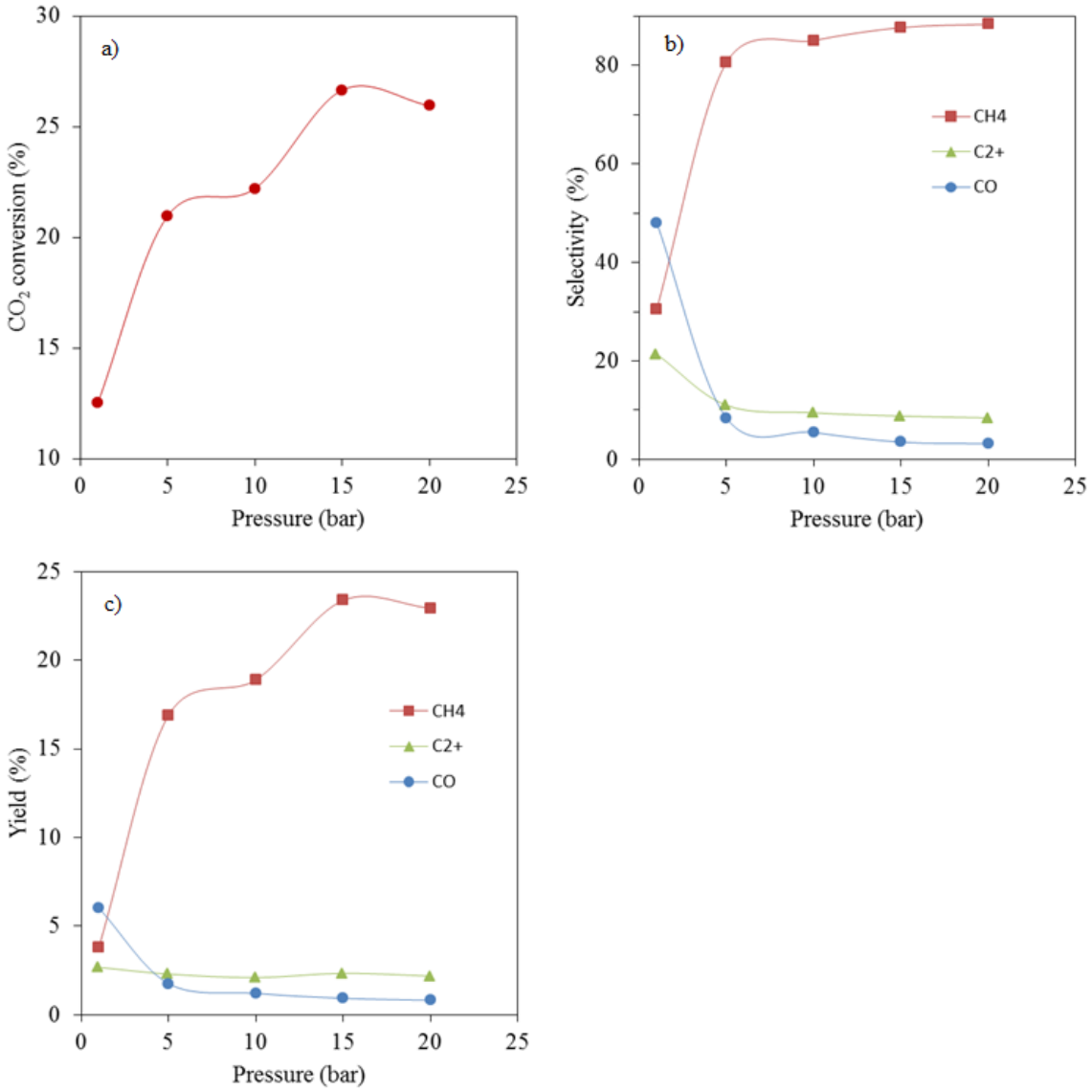

Figure 7. Effect of the operating pressure on (**a**) CO_2 conversion, (**b**) products selectivity and (**c**) products yields (catalyst—15%Co/3%K/SiO_2, 270 °C, SV = 0.92 NL/g_{cat}/h, H_2/CO_2 = 3.1/1).

2.6.3. Effect of Potassium Addition

Figure 8 shows the effect of potassium addition on CO_2 conversion, and products selectivity and yields. It is observed that the presence of potassium at a loading of as low as 1% results in a significant drop in CO_2 conversion from 39 to 16% when compared to the unpromoted catalyst (Figure 8a).

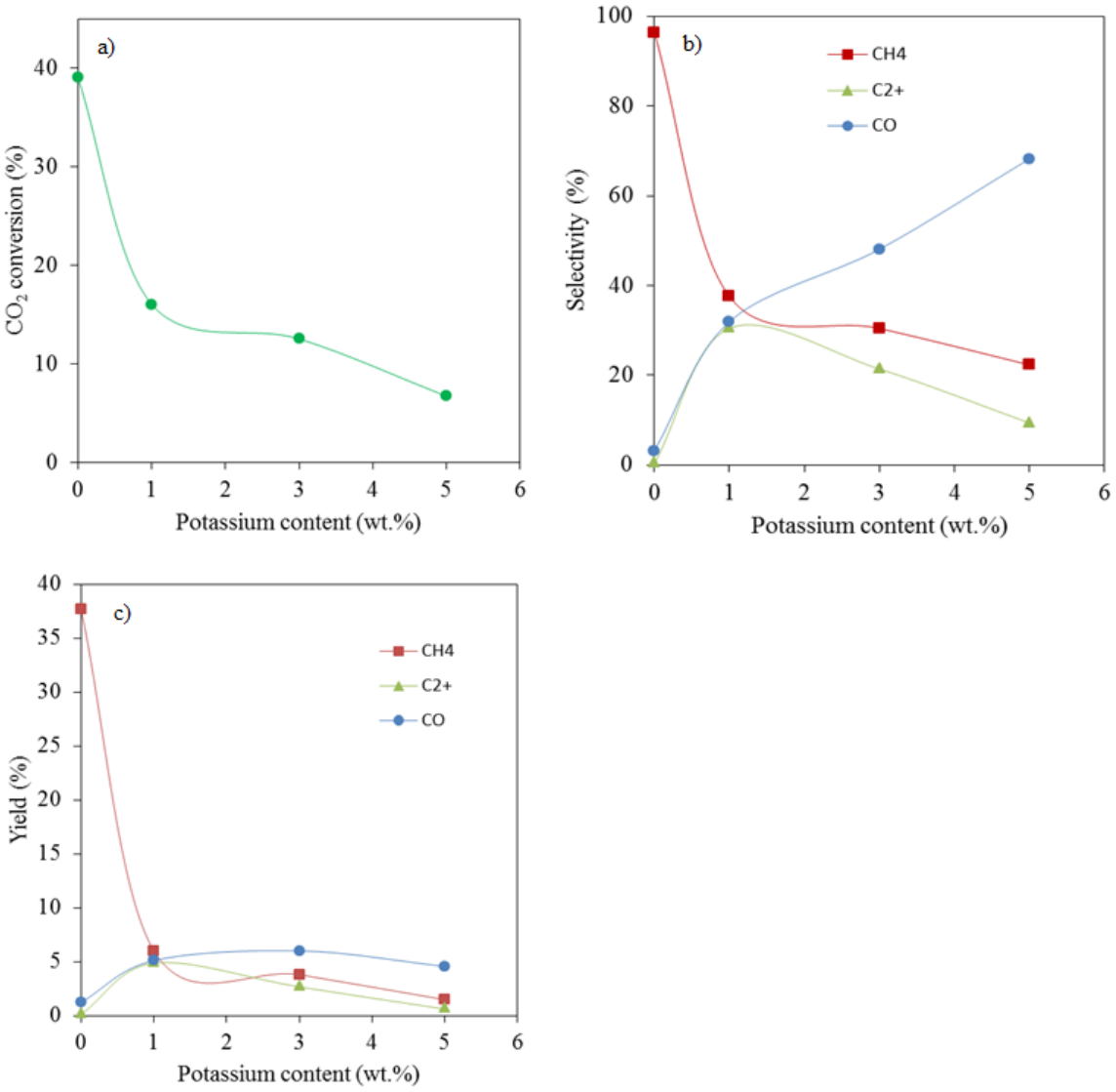

Figure 8. Effect of potassium loading on (**a**) CO_2 conversion, (**b**) product selectivity and (**c**) product yields.

Adding more potassium further exacerbates this behaviour, but with an attenuated effect. The following can explain these observations: (i) Coverage of active sites by potassium, although considered to happen at a low extent because of the low potassium loading employed; (ii) increase in CO_2 adsorption capacity: As discussed earlier in Section 2.4, CO_2-TPD results have shown that the CO_2 adsorption capacity for the catalyst improves upon potassium addition. As a consequence, the H/C molar ratio on the catalyst surface is decreased, leading to a drop in CO_2 conversion. This is in agreement with numerous experimental [30–33] and theoretical [34,35] investigations that reported a drop in CO_2 conversion with a decrease in H_2/CO_2 molar ratio. The decrease in CO_2 conversion with potassium addition was also reported by Owen et al. [13] and Shi et al. [8] on Co/SiO_2 and $CoCu/TiO_2$ catalysts, respectively. Using H_2 and CO_2 temperature-programmed desorption analyses, Shi et al. [8] were able to show that potassium promotion decreases the H_2 adsorption capacity of the catalyst, while that of CO_2 is enhanced; (iii) the oxidation state of cobalt in the catalyst: XRD results have shown the presence of CoO and metallic cobalt phases in all the reduced and passivated catalysts. TPR analyses, on the other hand, confirmed that these catalysts have different reducibility properties. Promotion with potassium limits the reducibility of the catalysts, resulting in limited amounts of metallic cobalt sites for CO_2 conversion. A similar relationship between catalyst reducibility and CO_2 activity was reported

by Melaet et al. [36] who conducted CO_2 hydrogenation on Co/SiO_2 catalysts activated at 523 K and 723 K. They established, by means of XPS, that CoO and metallic cobalt formed upon activation at 523 K and 723 K respectively. The catalyst reduced at 723 K showed higher activity.

The selectivity towards methane decreased from 96 to 37.6% (Figure 8b) upon adding 1 % of potassium to the catalyst. Meanwhile, the selectivity of both CO and C_{2+} hydrocarbons increased. Additional amounts of potassium resulted in a further decrease in methane selectivity and increase in CO selectivity. The selectivity of C_{2+} hydrocarbons, on the other hand, decreased with further increase in potassium loading above 1%. The improvement of C_{2+} hydrocarbons selectivity at 1% potassium can be attributed to a decreased surface H/C ratio as discussed earlier. This implies that carbon-containing species from CO_2 dissociation can polymerize rather than being hydrogenated as is often the case in a hydrogen-rich environment.

The decreased C_{2+} hydrocarbons selectivity at 3% and 5% potassium loading is also explained by an increased CO_2 adsorption capacity of the catalyst, causing a decrease in the surface H/C ratio. Since the CO yield is shown to increase and undergo little variations with further increase in potassium loading, while both CH_4 and the C_{2+} yields decrease (Figure 8c), it is possible that there is not enough surface hydrogen to readily react with both CO_2 and CO on the catalyst surface.

The highest C_{2+} yield achieved in this study was ca. 5% and was measured on the $15\%Co/1\%K/SiO_2$ catalyst at 1 bar and 270 °C. This condition is compared to results reported in other studies that used cobalt-based catalysts for CO_2 hydrogenation under various conditions, as summarized in Table 4. Of the catalysts that produced C_{5+} products at low pressure (<2 bar), our catalyst had the lowest methane selectivity under the optimized operating temperature and pressure. This is particularly important, since it offers opportunities to limit the formation of the undesirable methane without the need for excessive operating pressures that will make the process more energy-intensive.

3. Materials and Methods

3.1. Catalyst Synthesis

The catalyst synthesis consisted essentially of two steps, namely support preparation and metal loading. Fumed silica with an average particle size range of 0.2–0.3 µm, supplied by Sigma-Aldrich South Africa, served as the catalyst supporting material. Given its small particle size, it was pre-treated with deionized water and agglomerated by drying overnight at 120 °C in the air before crushing and sieving to obtain a powder with particles within the size range of 212–500 µm. The powder so obtained was subsequently calcined at 400 °C for 6 h in the air to lock its properties before loading the metals. The addition of cobalt and potassium was done through co-impregnation with solutions of cobalt and potassium nitrates—both purchased from Sigma-Aldrich. After impregnation, the catalysts were dried overnight at 120 °C and calcined at 400 °C in the air for 6 h. All the prepared catalysts contained 15 wt.% cobalt with varying potassium loading (0–5 wt.%). The amount of silica used in catalyst preparation was reduced to account for the addition of potassium. This allowed for the cobalt loading to be kept constant for all the catalysts.

Table 4. Summary of catalytic performance data for CO_2 hydrogenation over cobalt-based catalysts.

Entry	Catalyst	Prep. Method	H_2:CO_2	T [K]	P [bar]	SV	Conv. [%]	%Selectivity				References
								CH_4	CO	C_2+	C_{5+}	
1	100Co/5Cu	Coprecip.	3:1	473		0.2 L/gCat/h [a]						[12]
2	100Co/5Cu/2K_2CO_3	Coprecip.	3:1	498		0.16	49				1.12 [b]	
3	100Co/5Cu/2K_2CO_3	Coprecip.	3:1	498		0.16	56				2.32	
4	100Co/5Cu/2K_2CO_3	Coprecip.	3:1	473		0.16	40				1.91	
5	100Co/5Cu/2K_2CO_3	Coprecip.	3:1	498		0.16	22				2.81	
6	100Co/5Cu/2K_2CO_3	Coprecip.	3:1	473		0.16	10				0.19	
7	100Co/5Cu/2K_2CO_3	Coprecip.	3:1	473		0.16	44				1.59	
8	100Co/5Cu/5CeO_2/2K_2CO_3	Coprecip.	3:1	498		0.16	54				1.43	
9	100Co/5Cu/1CeO_2/2K_2CO_3	Coprecip.	2:1	498		0.15	34				2.11	
10	100Co/5Cu/1CeO_2	Coprecip.	2:1	498		0.15	40				0.10	
11	100Co/5Cu/1CeO_2/3K_3PO_4	Coprecip.	3:1	498		0.16	40				1.42	
12	100Co/5Cu/1CeO_2/4.5K_2CO_3/100MgO	Coprecip.	2:1	513		0.3	21				0.29	
13	100Co/5Cu/1CeO_2/4.5K_2CO_3/100MgO	Coprecip.	2:1	498		0.15	8				0.51	
14	100Co/5Cu/1CeO_2/6K_2CO_3/100H.S.C.	Coprecip.	2:1	518		0.15	19				2.71	
15	100Co/5Cu/100CeO_2/7K_2CO_3	Coprecip.	2:1	523		0.15	23				1.61	
16	100Co/5Cu/1CeO_2/4.5K_2CO_3/100F.C.	Coprecip.	2:1	513		0.075	23				0.24	
17	100Co/5Cu/1CeO_2/3.8K_2CO_3/50H.S.C.	Coprecip.	2:1	498		0.12	22				1.90	
18	3%Co/SiO_2	Impregnation	4:1, 95%N_2	500	1.4	4340/h	9.6	71	25	4.6		[23]
19				500		8480	6.5	54	35	11		
20				525		8480	12.3	59	33	8.2		
21				525		16,400	9.4	42	49	8.9		
22				550		16,400	13.7	42	52	5.9		
23				550		24,600	12	32	52	17		
24	15%Co/SiO_2	Impregnation	4:1, no N_2	476	1	2050–3850	10.5	86.9	12.6	0.7	0	
25				478	11	450–9620	11.2	89	10.7	0.34	0	
26	100%Co	Reduction	4:1	493	1	500–3000 h^{-1}	1.9	98	2			[25]
27	4.5%Co/S1	Impregnation		493			1.8	40	60			
28	4.6%Co/S3	Impregnation		493			6.3	66	34			
29	100 Co/60 MnO/147 SiO_2/0.15Pt	Precip. and Impregnation	2:1	463	10	30 mL/min/g of Co	18	95				[37]
30	15%Co/Al_2O_3	Impregnation	2.45:1	493	20	4800 cm^3(STP)/h/gcat	33	>90				[38]
31	20%Co/SSP	Impregnation	20:2	493	1	18 L/gcat/h	27	89.5	10.5			[39]
32	20%Co/MCM-41						28	91.4	8.6			
33	20%Co/TiSSP						16	92.1	7.9			
34	Co/TiMCM-41						34	94.9	5.1			
35	0.5% Pt–25% Co/γ-Al_2O_3	Impregnation	3:1	493	19.9	5.0 L/g cat/h		93.3		6.66	5.16	[28]
36	5%Co/Al_2O_3 [c]	Impregnation	6:1	533	1	13.5 mL/min/(63 to 70 mg of cat)	0.21	35.7				[40]
37	10%Co/Al_2O_3 [c]						0.91	74.2				
38	15%Co/Al_2O_3 [c]						2.45	87.8				
39	20%Co/Al_2O_3 [c]						2.1	85.7				
40	Co/Al_2O_3	Solid state reaction of gibbsite and CoNT	10:1	543	1	150 mL/min/gcat	76	82.2	17.8			[41]

Table 4. *Cont.*

Entry	Catalyst	Prep. Method	H_2:CO_2	T [K]	P [bar]	SV	Conv. [%]	%Selectivity				References
41	Co/Al_2O_3	Solid state reaction of gibbsite and CoAc					48.7	76.7	23.3			
42	Co/Al_2O_3	Solid state reaction of gibbsite and CoAA					20.3	76.4	23.6			
43	Co/Al_2O_3	Solid state reaction of gibbsite and CoCL					6.1	100	0			
44	Co/Al_2O_3	Impregnation using CoNT					32.2	86.5	13.5			
45	20%Co/SiO_2		3:1	643	Atmospheric		67.4	95.3	4.2	0.6	0	[13]
46	20%Co/1%Pd/SiO_2						50.7	93.4	6.3	0.3	0	
47	10%Co/1%Pd/1%K/SiO_2						36.4	89.3	8.0	2.8	0	
48	20%Co/1%Pd/1%K/SiO_2						63.4	80.3	13.9	5.9	0	
49	10%Co/1%Pd/1%K/SiO_2						39.1	82.9	9.5	7.6	0.09	
50	20%Co/1%Pd/0.5%K/SiO_2						62.8	76.0	15.3	8.8	0	
51	20%Co/1%Pd/1.5%K/SiO_2						59.1	64.7	16.2	19.1	1.26	
52	20%Co/1%Pd/3%K/SiO_2						43.2	53.1	24.3	22.6	2.73	
53	20%Co/1%K/SiO_2						36.1	45.3	16.9	37.8	7.87	
54	20%Co/1%Pt/1%K/SiO_2						36.5	41.5	20.8	37.7	9.58	
55	20%Co/1%Ru/1%K/SiO_2						45.1	52.6	12.6	34.8	5.68	
56	20%Co/1%Pd/1%Li/SiO_2						39.5	56.1	19.2	24.6	1.94	
57	20%Co/1%Pd/1%Na/SiO_2						41.9	48.4	20.3	31.3	7.33	
58	20%Co/1%Li/SiO_2						39.3	58.4	21.4	20.2	0.47	
59	20%Co/1%Na/SiO_2						51.2	42.1	21.7	36.3	5.01	
60	20%Co/1%K/SiO_2						47.6	50.1	17.0	32.9	3.65	
61	20%Co/1%Mo/SiO_2						64.8	88.7	6.5	4.8	0	
62	20%Co/1%Cr/SiO_2						60.9	75.9	22.8	1.2	0	
63	20%Co/1%Mn/SiO_2						62	91.1	6.9	2.0	0	
64	20%Co/1%Na/1%Mn/SiO_2						42.7	58.2	19.7	22.2	0.80	
65	20%Co/1%Na/1%Mo/SiO_2						43.9	38.3	15.7	45.9	8.76	
66	$CoCu/TiO_2$	Deposition-precipitation	73:24	523	50	3000 mL/g/h	23.1	87.0	1.3	10.2	4.76	[8]
67	1.5 K–$CoCu/TiO_2$						21.2	59.3	4.7	36.5	13.21	
68	2.0 K–$CoCu/TiO_2$						13.8	37.1	19.7	44.6	17.39	
69	2.5 K–$CoCu/TiO_2$						13	22.4	35.1	43.3	23.08	
70	3.0 K–$CoCu/TiO_2$						12.8	21.9	35.9	41.5	19.53	
71	3.5 K–$CoCu/TiO_2$						11.9	18.9	45.9	35.1	16.81	
72	15%Co-1%K/SiO_2	Impregnation	3:1	543	1 bar	0.92 NL/gcat/h	16	37.6	31.9	30.5	7.8	This study

[a] Calculated from reported flow of CO_2 over 24 h, H_2/CO_2 ratio and the mass of catalyst. [b] Calculated from the reported milliliters of oil that formed during the reaction, assuming an average chain length of 7 (density of 0.684). [c] Data read from graphs.

3.2. Catalyst Characterization

The surface area and the porosity of the catalysts were measured by nitrogen physisorption at −196 °C using an Accelerated Surface Area and Porosimetry System (ASAP 2460) from Micromeritics. Each analysis was preceded by degassing the sample at 150 °C for 4 h. The multipoint Brunauer-Emmett-Teller (BET) method was used to determine the surface area of the materials analysed.

The reducibility of the catalysts was studied by means of temperature-programmed reduction (TPR). An in-house built instrument, equipped with a thermal conductivity detector (TCD), was used for this purpose. In a typical analysis, 100 mg of catalyst was loaded in a stainless-steel reactor and heated to 300 °C for one hour under 70 NmL/min of helium to remove traces of moisture and other ambient contaminants. This step was referred to as degassing. After allowing the reactor to cool to room temperature, helium was switched with a gas mixture containing 5% H_2 in argon at a flow of 65 NmL/min. In the final step, the temperature was raised from room temperature to 700 °C at a heating rate of 10 °C/min, while recording the signal of the TCD.

Temperature-programmed desorption (TPD) of CO_2 was carried out using the same instrument as described for TPR analysis. Different to TPR analysis, the catalysts used in this analysis were first reduced at 335 °C for 17 h, using the same reactor and conditions as for the reduction of catalyst samples used in the CO_2 hydrogenation testing as will be described in Section 2.3. The reduced catalysts were passivated using 5% O_2 in helium for 2 h at ambient temperature before their transfer from the CO_2 hydrogenation reactor to the TPD apparatus. Two hundred milligrams of catalyst sample was degassed in a similar manner as for TPR analysis. After degassing and cooling to room temperature, the temperature was raised to 335 °C at a heating rate of 10 °C/min and maintained at this value for 30 min under a flow of 5% H_2 in argon. This step was necessary for the removal of the cobalt oxide layer formed during catalyst passivation. Thereafter, the reactor was cooled and maintained at 50 °C for at least 10 min before replacing H_2 (5% in argon) with CO_2 (10% in helium). CO_2 adsorption was performed at 50 °C for 1 h before re-introducing helium, but this time to remove the physically adsorbed CO_2 molecules. TPD was then performed under helium flow, after stabilization of the TCD signal, from 50 to 700 °C at a heating rate of 5 °C/min.

X-ray diffraction (XRD) analysis was performed to identify the oxidation state of cobalt species in the unreduced and reduced catalyst samples. The instrument used for this purpose was a Rigaku Ultima IV equipped with a copper target. The voltage and current at which the diffractometer was operated were 40 kV and 30 mA respectively. Spectra were acquired in the range of 2θ from 10° to 90° with a step size of 0.01° at the scanning speed of 1°/min.

X-ray photoelectron spectroscopy (XPS) was used to determine the oxidation states of the elements present on the surface of the catalysts. This analysis was performed on a Specs Phoibos 150 spectrometer with a monochromatic X-ray source Al Kα at 1486.71 eV. A low-energy electron flood gun operated at 2.0–2.5 eV and 20 μA was used to stabilize the sample surface charge. The spectrometer was operated at constant pass energy of 40 eV. The shift in binding energy peaks position, due to the surface charging effect was corrected by setting the C 1s binding energy to 284.8 eV [14].

3.3. Catalyst Testing

Carbon dioxide hydrogenation was carried out in a system which consisted mainly of a stainless steel fixed-bed reactor (16 mm i.d. × 220 mm length) mounted in an electrical furnace, a mass flow controller (Aalborg), a back-pressure regulator and a product collection pot. The furnace temperature was controlled using a programmable temperature controller connected to a K-type thermocouple and the furnace heating element. Accurate reaction temperatures were measured by means of another K-type thermocouple in direct contact with the catalyst bed held in place by plugs of quartz wool. Any liquid product formed was collected in a cold pot mounted at the bottom of the reactor. There was no need for a hot trap since the products were mainly light hydrocarbons. The reactor outlet was connected to a three-way valve, which made it possible to either send the reaction products to vent or to an online gas chromatograph (GC) for analysis. The Dani Master GC used in this study was

equipped with a flame ionization detector (FID) connected to a capillary column (Supel-Q^{TM} PLOT) that separated hydrocarbons and oxygenates, and a thermal conductivity detector (TCD) connected to a packed column (60/80 Carboxen 1000) for the separation of H_2, N_2, CO and CO_2.

Prior to testing, 500 mg of catalysts were reduced in flowing hydrogen (23 NmL/min) at 335 °C and atmospheric pressure for 17 h. Catalyst testing was done at temperatures ranging from 180 to 300 °C with an increment of 15 °C and at pressures within a range of 1–20 bar at a space velocity of 0.92 NL/g_{cat}/h. The feed gas was premixed and contained 21.8% CO_2, 68.6% H_2 and 9.6% N_2. After testing, all catalysts were passivated in 5% O_2 in helium (23 NmL/min) at room temperature for 2 h. The nitrogen present in the feed gas was used as an internal standard for mass balance calculations. The CO_2 conversion, the rate of CO_2 conversion, the rate of products formation, selectivity and yield were calculated according to Equations (1)–(5), where F and X indicate the total molar gas flow rate and mole fraction respectively. The subscripts "in" and "out" refer to the gas streams entering or leaving the reactor.

$$CO_2 \text{ conversion } (\%) = \frac{X_{CO_2,\text{ in}} - \frac{X_{N_2,\text{ in}}}{X_{N_2,\text{ out}}} \times X_{CO_2,\text{ out}}}{X_{CO_2,\text{in}}} \times 100, \quad (1)$$

$$\text{Rate of } CO_2 \text{ conversion } = \frac{F_{in}\left[X_{CO_2,\text{ in}} - \frac{X_{N_2,\text{ in}}}{X_{N_2,\text{ out}}} \times X_{CO_2,\text{ out}}\right]}{\text{Catalyst mass}}, \quad (2)$$

$$\text{Rate of formation of product i } = \frac{F_{out} \times X_{i,\text{ out}}}{\text{Catalyst mass}}, \quad (3)$$

$$\text{Selectivity of product i } (\%) = \frac{\text{moles of carbon in product i per unit time}}{\text{Rate of } CO_2 \text{ conversion } \times \text{ Catalyst mass}} \times 100, \quad (4)$$

$$\text{Yield of product i } (\%) = \frac{\text{Selectivity of product i } \times \text{ } CO_2 \text{ conversion}}{100}. \quad (5)$$

After a change in operating conditions or in catalyst sample, the reactor was allowed to reach a steady state and maintained at the new conditions for at least two days. At least two data points were generated per day. To ensure reproducibility, each data point was an average of three independent measurements that were closer to each other within 5% error range.

4. Conclusions

The aim of this study was to investigate the effects of operating conditions (temperature, pressure) and potassium loading on the performance of silica-supported cobalt catalysts in CO_2 hydrogenation. The highest yield in C_{2+} hydrocarbons was measured at 1 bar and 270 °C. Potassium was found to negatively affect the reducibility of the catalyst, while enhancing its CO_2 adsorption capacity. The improved CO_2 adsorption capacity of the catalyst leads to a lower surface H/C ratio, which promotes chain growth reactions. The limited catalyst reducibility resulted in low catalyst activity and is explained by an electric donation of potassium to cobalt species during the calcination process of the catalyst. The optimal operating pressure and temperature determined in this study, combined with catalyst promotion with 1 wt.% of potassium, significantly lowered the undesirable methane selectivity when compared to other cobalt-based catalysts that also produced some C_{5+} hydrocarbons at low pressures (<2 bar). This constitutes a significant further step in the development of efficient catalysts for CO_2 hydrogenation to liquid fuels.

Author Contributions: Project conceptualization and methodology: R.A.I. and K.J.; Materials synthesis, experiments and data collection: R.A.I.; Data analysis and interpretation: R.A.I. and K.J.; Manuscript writing and editing: R.A.I. and K.J.; Project administration and supervision: K.J.

Funding: This project was funded by the National Research Foundation (Grant: UID 90757) and the University of Johannesburg Global Excellence Stature (GES) program.

Conflicts of Interest: The authors declare no conflicts of interest.

References

1. Espinal, R.; Taboada, E.; Molins, E.; Chimentao, R.J.; Medina, F.; Llorca, J. Cobalt hydrotalcites as catalysts for bioethanol steam reforming. The promoting effect of potassium on catalyst activity and long-term stability. *Appl. Catal. B Environ.* **2012**, *127*, 59–67. [CrossRef]
2. Xie, X.; Yin, H.; Dou, B.; Huo, J. Characterization of a potassium-promoted cobalt-molybdenum/alumina water-gas shift catalyst. *Appl. Catal.* **1991**, *77*, 187–198. [CrossRef]
3. Asano, K.; Ohnishi, C.; Iwamoto, S.; Shioya, Y.; Inoue, M. Potassium-doped Co_3O_4 catalyst for direct decomposition of N_2O. *Appl. Catal. B Environ.* **2008**, *78*, 242–249. [CrossRef]
4. Trépanier, M.; Tavasoli, A.; Dalai, A.K.; Abatzoglou, N. Co, Ru and K loadings effects on the activity and selectivity of carbon nanotubes supported cobalt catalyst in Fischer–Tropsch synthesis. *Appl. Catal. A Gen.* **2009**, *353*, 193–202. [CrossRef]
5. Tavasoli, A.H.M.A.D.; Khodadadi, A.; Mortazavi, Y.; Sadaghiani, K.; Ahangari, M.G. Lowering methane and raising distillates yields in Fischer–Tropsch synthesis by using promoted and unpromoted cobalt catalysts in a dual bed reactor. *Fuel Process. Technol.* **2006**, *87*, 641–647. [CrossRef]
6. Jacobs, G.; Das, T.K.; Zhang, Y.; Li, J.; Racoillet, G.; Davis, B.H. Fischer–Tropsch synthesis: Support, loading, and promoter effects on the reducibility of cobalt catalysts. *Appl. Catal. A Gen.* **2002**, *233*, 263–281. [CrossRef]
7. Calafat, A.; Vivas, F.; Brito, J.L. Effects of phase composition and of potassium promotion on cobalt molybdate catalysts for the synthesis of alcohols from CO_2 and H_2. *Appl. Catal. A Gen.* **1998**, *172*, 217–224. [CrossRef]
8. Shi, Z.; Yang, H.; Gao, P.; Li, X.; Zhong, L.; Wang, H.; Liu, H.; Wei, W.; Sun, Y. Direct conversion of CO_2 to long-chain hydrocarbon fuels over K–promoted CoCu/TiO_2 catalysts. *Catal. Today* **2018**, *311*, 65–73. [CrossRef]
9. Petala, A.; Panagiotopoulou, P. Methanation of CO_2 over alkali-promoted Ru/TiO_2 catalysts: I. Effect of alkali additives on catalytic activity and selectivity. *Appl. Catal. B Environ.* **2018**, *224*, 919–927. [CrossRef]
10. Panagiotopoulou, P. Methanation of CO_2 over alkali-promoted Ru/TiO_2 catalysts: II. Effect of alkali additives on the reaction pathway. *Appl. Catal. B Environ.* **2018**, *236*, 162–170. [CrossRef]
11. Numpilai, T.; Witoon, T.; Chanlek, N.; Limphirat, W.; Bonura, G.; Chareonpanich, M.; Limtrakul, J. Structure–activity relationships of Fe-Co/K-Al_2O_3 catalysts calcined at different temperatures for CO_2 hydrogenation to light olefins. *Appl. Catal. A Gen.* **2017**, *547*, 219–229. [CrossRef]
12. Russell, W.W.; Miller, G.H. Catalytic hydrogenation of carbon dioxide to higher hydrocarbons. *J. Am. Chem. Soc.* **1950**, *72*, 2446–2454. [CrossRef]
13. Owen, R.E.; O'Byrne, J.P.; Mattia, D.; Plucinski, P.; Pascu, S.I.; Jones, M.D. Cobalt catalysts for the conversion of CO_2 to light hydrocarbons at atmospheric pressure. *Chem. Commun.* **2013**, *49*, 11683–11685. [CrossRef] [PubMed]
14. Ernst, B.; Bensaddik, A.; Hilaire, L.; Chaumette, P.; Kiennemann, A. Study on a cobalt silica catalyst during reduction and Fischer-Tropsch reaction: In situ EXAFS compared to XPS and XRD. *Catal. Today* **1998**, *39*, 329–341. [CrossRef]
15. Huffman, G.P.; Shah, N.; Zhao, J.M.; Huggins, F.E.; Hoost, T.E.; Halvorsen, S.; Goodwin, J.G. In-situ XAFS investigation of K-promoted Co catalysts. *J. Catal.* **1995**, *151*, 17–25. [CrossRef]
16. De la Osa, A.; De Lucas, A.; Valverde, J.L.; Romero, A.; Monteagudo, I.; Coca, P.; Sánchez, P. Influence of alkali promoters on synthetic diesel production over Co catalyst. *Catal. Today* **2011**, *167*, 96–106. [CrossRef]
17. Biesinger, M.C.; Payne, B.P.; Grosvenor, A.P.; Lau, L.W.; Gerson, A.R.; Smart, R.S.C. Resolving surface chemical states in XPS analysis of first row transition metals, oxides and hydroxides: Cr, Mn, Fe, Co and Ni. *Appl. Surf. Sci.* **2011**, *257*, 2717–2730. [CrossRef]
18. Hu, X.; Dong, D.; Shao, X.; Zhang, L.; Lu, G. Steam reforming of acetic acid over cobalt catalysts: Effects of Zr, Mg and K addition. *Int. J. Hydrog. Energy* **2017**, *42*, 4793–4803. [CrossRef]
19. Kono, E.; Tamura, S.; Yamamuro, K.; Ogo, S.; Sekine, Y. Pd/K/Co-oxide catalyst for water gas shift. *Appl. Catal. A Gen.* **2015**, *489*, 247–254. [CrossRef]
20. Petitto, S.C.; Langell, M.A. Surface composition and structure of Co_3O_4 (110) and the effect of impurity segregation. *J. Vac. Sci. Technol. A* **2004**, *22*, 1690–1696. [CrossRef]
21. Melaet, G.; Lindeman, A.E.; Somorjai, G.A. Cobalt particle size effects in the Fischer–Tropsch synthesis and in the hydrogenation of CO_2 studied with nanoparticle model catalysts on silica. *Top. Catal.* **2014**, *57*, 500–507. [CrossRef]

22. Iablokov, V.; Beaumont, S.K.; Alayoglu, S.; Pushkarev, V.V.; Specht, C.; Gao, J.; Alivisatos, A.P.; Kruse, N.; Somorjai, G.A. Size-controlled model Co nanoparticle catalysts for CO_2 hydrogenation: Synthesis, characterization, and catalytic reactions. *Nano Lett.* **2012**, *12*, 3091–3096. [CrossRef] [PubMed]
23. Weatherbee, G.D.; Bartholomew, C.H. Hydrogenation of CO_2 on group VIII metals: IV. Specific activities and selectivities of silica-supported Co, Fe, and Ru. *J. Catal.* **1984**, *87*, 352–362. [CrossRef]
24. Mutschler, R.; Moioli, E.; Luo, W.; Gallandat, N.; Züttel, A. CO_2 hydrogenation reaction over pristine Fe, Co, Ni, Cu and Al_2O_3 supported Ru: Comparison and determination of the activation energies. *J. Catal.* **2018**, *366*, 139–149. [CrossRef]
25. Guerrero-Ruiz, A.; Rodriguez-Ramos, I. Hydrogenation of CO_2 on carbon-supported nickel and cobalt. React. Kinet. *Catal. Lett.* **1985**, *29*, 93–99. [CrossRef]
26. Fernández-Morales, I.; Guerrero-Ruiz, A.; López-Garzón, F.J.; Rodríguez-Ramos, I.; Moreno-Castilla, C. Hydrogenolysis of n-butane and hydrogenation of carbon monoxide on Ni and Co catalysts supported on saran carbons. *Appl. Catal.* **1985**, *14*, 159–172. [CrossRef]
27. Yao, Y.; Hildebrandt, D.; Glasser, D.; Liu, X. Fischer−Tropsch synthesis using H2/CO/CO2 syngas mixtures over a cobalt catalyst. *Ind. Eng. Chem. Res.* **2010**, *49*, 11061–11066. [CrossRef]
28. Gnanamani, M.K.; Shafer, W.D.; Sparks, D.E.; Davis, B.H. Fischer–Tropsch synthesis: Effect of CO_2 containing syngas over Pt promoted Co/γ-Al_2O_3 and K-promoted Fe catalysts. *Catal. Commun.* **2011**, *12*, 936–939. [CrossRef]
29. Habazaki, H.; Yamasaki, M.; Zhang, B.P.; Kawashima, A.; Kohno, S.; Takai, T.; Hashimoto, K. Co-methanation of carbon monoxide and carbon dioxide on supported nickel and cobalt catalysts prepared from amorphous alloys. *Appl. Catal. A Gen.* **1998**, *172*, 131–140. [CrossRef]
30. Dorner, R.W.; Hardy, D.R.; Williams, F.W.; Davis, B.H.; Willauer, H.D. Influence of Gas Feed Composition and Pressure on the Catalytic Conversion of CO_2 to Hydrocarbons Using a Traditional Cobalt-Based Fischer-Tropsch Catalyst. *Energy Fuels* **2009**, *23*, 4190–4195. [CrossRef]
31. Gnanamani, M.K.; Jacobs, G.; Shafer, W.D.; Sparks, D.; Davis, B.H. Fischer–Tropsch synthesis: Deuterium kinetic isotope study for hydrogenation of carbon oxides over cobalt and iron catalysts. *Catal. Lett.* **2011**, *141*, 1420–1428. [CrossRef]
32. Fröhlich, G.; Kestel, U.; Łojewska, J.; Łojewski, T.; Meyer, G.; Voß, M.; Borgmann, D.; Dziembaj, R.; Wedler, G. Activation and deactivation of cobalt catalysts in the hydrogenation of carbon dioxide. *Appl. Catal. A Gen.* **1996**, *134*, 1–19. [CrossRef]
33. Lahtinen, J.; Anraku, T.; Somorjai, G.A. C, CO and CO_2 hydrogenation on cobalt foil model catalysts: Evidence for the need of CoO reduction. *Catal. Lett.* **1994**, *25*, 241–255. [CrossRef]
34. Torrente-Murciano, L.; Mattia, D.; Jones, M.D.; Plucinski, P.K. Formation of hydrocarbons via CO_2 hydrogenation–A thermodynamic study. *J. CO_2 Util.* **2014**, *6*, 34–39. [CrossRef]
35. Gao, J.; Wang, Y.; Ping, Y.; Hu, D.; Xu, G.; Gu, F.; Su, F. A thermodynamic analysis of methanation reactions of carbon oxides for the production of synthetic natural gas. *RSC Adv.* **2012**, *2*, 2358–2368. [CrossRef]
36. Melaet, G.; Ralston, W.T.; Li, C.S.; Alayoglu, S.; An, K.; Musselwhite, N.; Kalkan, B.; Somorjai, G.A. Evidence of highly active cobalt oxide catalyst for the Fischer–Tropsch synthesis and CO_2 hydrogenation. *J. Am. Chem. Soc.* **2014**, *136*, 2260–2263. [CrossRef] [PubMed]
37. Riedel, T.; Claeys, M.; Schulz, H.; Schaub, G.; Nam, S.-S.; Jun, K.-W.; Choi, M.-J.; Kishan, G.; Lee, K.-W. Comparative study of Fischer–Tropsch synthesis with H_2/CO and H_2/CO_2 syngas using Fe- and Co-based catalysts. *Appl. Catal. A Gen.* **1999**, *186*, 201–213. [CrossRef]
38. Visconti, C.G.; Lietti, L.; Tronconi, E.; Forzatti, P.; Zennaro, R.; Finocchio, E. Fischer–Tropsch synthesis on a Co/Al_2O_3 catalyst with CO_2 containing syngas. *Appl. Catal. A Gen.* **2009**, *355*, 61–68. [CrossRef]
39. Janlamool, J.; Praserthdam, P.; Jongsomjit, B. Ti-Si composite oxide-supported cobalt catalysts for CO_2 hydrogenation. *J. Nat. Gas Chem.* **2011**, *20*, 558–564. [CrossRef]

40. Das, T.; Deo, G. Synthesis, characterization and in situ DRIFTS during the CO_2 hydrogenation reaction over supported cobalt catalysts. *J. Mol. Catal. A Chem.* **2011**, *350*, 75–82. [CrossRef]
41. Srisawad, N.; Chaitree, W.; Mekasuwandumrong, O.; Shotipruk, A.; Jongsomjit, B.; Panpranot, J. CO_2 hydrogenation over Co/Al_2O_3 catalysts prepared via a solid-state reaction of fine gibbsite and cobalt precursors. *React. Kinet. Mech. Catal.* **2012**, *107*, 179–188. [CrossRef]